IET Power Electronics

Research Article

IET Journals
The Institution of Engineering and Technology

Improved control algorithm for grid-connected cascaded H-bridge photovoltaic inverters under asymmetric operating conditions

ISSN 1755-4535
Received on 16th December 2016
Revised 19th July 2017
Accepted on 29th July 2017
E-First on 18th January 2018
doi: 10.1049/iet-pel.2016.0983
www.ietdl.org

Hossein Iman-Eini[1] ✉, *Seddik Bacha*[2], *David Frey*[2]

[1]*School of Electrical and Computer Engineering, College of Engineering, University of Tehran, Tehran, Iran*
[2]*Grenoble Electrical Engineering Laboratory, University of Grenoble Alpes, Grenoble, France*
✉ *E-mail: imaneini@ut.ac.ir*

Abstract: Here, a single-stage cascaded H-bridge (CHB) inverter is presented for grid-connected photovoltaic (PV) systems. The CHB inverter has separate DC links and allows individual control of PV arrays. The conversion efficiency is high and the harmonic generation is lower than conventional PV inverters. Although the CHB inverter is a good candidate for injection of solar power into grid, its control issues have not been completely solved. One of the main challenges in the CHB inverter is the harmonic generation when the connected PV arrays to the H-bridge cells have different amounts of insolation. This study deals with the asymmetrical operating conditions of PV arrays (or H-bridge cells) in the CHB inverter and presents an analytical equation for determination of cells' modulation indices based on PV arrays data. Then, a control loop is added to the tracking algorithm of conventional control systems to determine whether an H-bridge cell is in the linear modulation or not. In the case of overmodulation, the corresponding DC link voltage is increased by the controller to bring it back to the linear region. The validity of new method is confirmed by simulations and experiments on a seven-level 1.7 kW CHB inverter.

1 Introduction

In the last decade, the multilevel inverters have gained a lot of attention in the industry due to their salient features such as lower harmonic generation, lower electromagnetic interference generation, smaller output filters, and improved current quality [1]. Among these topologies, the cascaded H-bridge (CHB) inverter is especially interesting for photovoltaic (PV) applications. It needs the minimum number of components for synthesising the same number of voltage levels. It also provides several distinct DC links (Fig. 1) which allows the independent control of PV arrays [2, 3]. Then, by employing a sophisticated control system, the maximum power point (MPP) of each string can be controlled independently [4]. In addition, the CHB inverter can process the electric power in one stage, which results in a higher conversion efficiency.

The control of CHB-based PV inverter is simple if the connected PV arrays to the H-bridge cells are similar and have identical operating conditions. However, as the solar insolation of individual PV arrays (or input power to the H-bridge cells) becomes different, for example, due to partial shading or mismatch of PV arrays, the classic control fails to operate correctly [5, 6]. In such operating conditions, the generated power by the PV arrays are different and the CHB inverter may enter to the overmodulation region.

Several control techniques have been introduced for the control of grid-connected CHB inverters [7–13]. In [7], a controller based on fuzzy approach has been introduced which integrates the control system with the modulator. Kouro *et al*. [8] have proposed a simple method to handle mismatching between the H-bridge cells by controlling the cells' modulation indices. This approach employs a feedforward term in the modulation stage to control the drift of DC-link voltages. The inter-phase power imbalance in the three-phase CHB inverters has been addressed in [9]. To solve the problem, a zero sequence voltage is imposed upon the phase legs in order to affect the current flowing into each phase. The cascade connection of three-phase cells has been introduced in [10]. It regulates the voltage of PV arrays to a predefined constant voltage. This method, however, fails to track the MPP of PV strings when the irradiance level changes. Farivar *et al*. [11] have introduced a method to reduce the number of PV sensors in the CHB inverter. The control system monitors the waveform of ac terminal, before and after each switching transition. Then, the voltage of each DC link is estimated and is used in the tracking algorithm. This technique, however, should employ a very low update frequency, i.e. a few hertz for the MPPT goal which limits its usage in many applications. In [12], based on energy balance between the H-bridge cells and the grid, a control method is proposed which ensures the stability of CHB inverter around a wide range of operating points. In [13], a model predictive control method is proposed, where the predictions for each switching state are calculated and evaluated in a cost function in order to find the best control action. The last two references use a parameter-based control method and their performance will deteriorate when the parameters of the system change.

A few methods have evaluated the behaviour of the CHB inverter under heavy mismatching conditions, where the inverter enters to the overmodulation region [14–17]. In [14], power factor of the inverter is used as a freedom degree to keep the inverter in the linear modulation range. In this method, however, an uncontrolled amount of reactive power is injected to (or absorbed from) the grid. In [15], the control system shifts the operating point of H-bridge cells when they enter to the overmodulation region. However, there is no experimental verification and the operating principle has not been generalised. In [16], a similar idea as [15] has been introduced and experimental results have been given for a scaled down 80 V system. This reference, however, does not provide any analysis about the effect of voltage increase on the system output. In addition, the total harmonic distortion (THD) of injected current to the grid is higher than 5% which is not satisfactory. Miranbeigi and Iman-Eini [17] present a control method based on the derivative of power with respect to array current for single-phase CHB inverters. Implementation of this method, however, needs careful considerations in practice to reduce the effect of environmental noises on the system performance. In [18, 19], the idea of two-stage PV converters based on CHB inverters has been introduced. This type of converter employs DC/DC converters for the MPPT of PV arrays. However, by employing the DC–DC converters, the overall

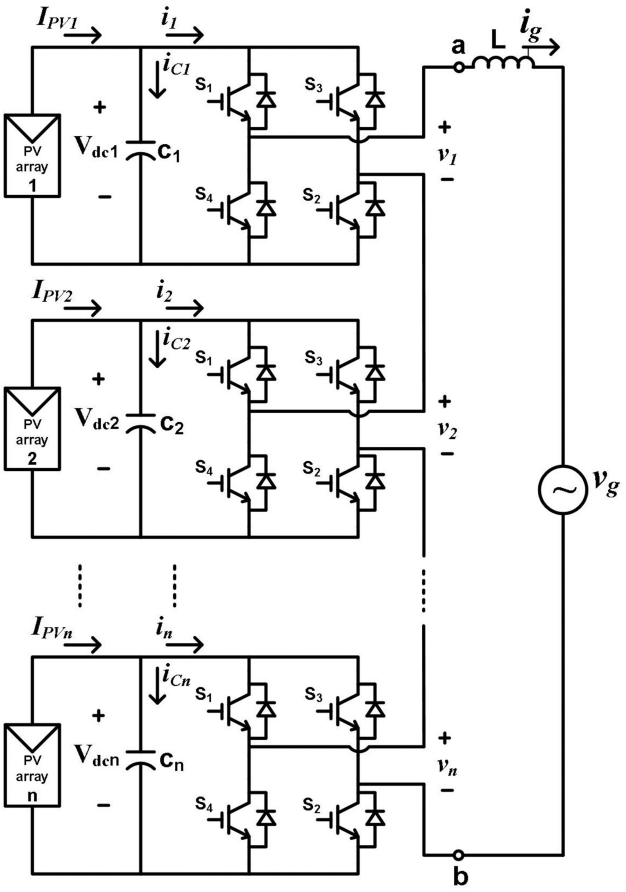

Fig. 1 *Grid-connected PV inverter based on the CHB inverter*

efficiency of the system reduces by 4–10% and the cost and complexity of the system increases [11, 20].

In contrast to [15, 16] which have been developed for a seven-level CHB inverter, this paper extends the idea of DC link voltage increase under asymmetric operating conditions for a CHB inverter with an arbitrary number of H-bridge cells. Based on mathematical and circuit analysis, analytical relations are derived for the evaluation of H-bridge cells. Using these formulas, one can recognise whether an H-bridge cell is in the linear modulation range or not. Then, a control loop is added to the tracking algorithm to evaluate the condition of H-bridge cells. In the condition that one H-bridge cell enters to the overmodulation region, its reference voltage is increased gradually to bring it back to the linear range; otherwise, the reference voltage is updated by the MPPT algorithm. The procedure of selecting the step voltage and the update frequency of MPPT algorithm to meet the control goals are explained. The effect of voltage increase on the system output is also evaluated analytically. Moreover, the dynamic behaviour of the control system is investigated by simulations. Finally, the claims are verified by simulations and experiments on a seven-level 1.7 kW CHB inverter.

2 CHB-based PV inverter

Fig. 1 demonstrates the structure of a single-phase CHB inverter as a grid-connected PV inverter. This structure is completely modular and is made of n series-connected H-bridge cells. Each H-bridge has four power switches and a DC link capacitor represented by C_j ($j = 1,2,\ldots,n$). Each capacitor is connected to a separate PV array and helps to reduce the voltage ripple. Moreover, each H-bridge cell can synthesise '0', '$+V_{\rm dc}$', and '$-V_{\rm dc}$' at its ac terminals, which is defined by v_j ($j = 1, 2,\ldots, n$) and the inverter phase voltage v_{ab} is equal to the sum of ac terminal voltages, i.e. $v_{ab} = \sum_{j=1}^{n} v_j$. Using n H-bridge cells, $2n + 1$ voltage levels can be synthesised at the ac terminal. An inductor is also placed between the inverter and the grid to shape the inductor current $i_{\rm g}$.

In [21], different modulation algorithms have been introduced for the CHB inverter. Among these methods, the phase-shifted PWM (PS-PWM) has a simple structure and the distribution of power loss among the power switches is uniform. In addition, the effective switching frequency is n times of the PWM carrier frequency. Hence, this modulation technique is employed for synthesising v_{ab} in this paper.

3 Proposed control system for the CHB inverter

In this section, first the standard limit on the harmonic generation of a PV inverter is stated. Then, a mathematical equation which relates the operating condition of an H-bridge cell to the harmonic generation (or its modulation index) is derived. Next, the proposed control system is introduced.

3.1 Derivation of cells' modulation indices based on PV system data

For grid-connected PV inverters, the current distortion level is one important power quality index. It is stated in both the IEEE Std 1547-2003 and the IEC Standard 61727 that the THD for the grid current should be lower than 5% to avoid adverse effects on the other consumers and the grid [22]. To satisfy this requirement, the current controller should be properly designed and the inverter must work in the linear modulation range.

In the CHB inverter shown in Fig. 1, there are n series-connected H-bridge cells at the ac side. For evaluation of inverter behaviour, the modulation index of all H-bridge cells should be considered. In this regard, the modulation index of jth H-bridge cell is written as

$$m_j = \frac{V_j^1}{V_{{\rm dc}j}}, \quad j = 1, 2, \ldots, n \tag{1}$$

where m_j represents the modulation index of jth H-bridge cell, $V_{{\rm dc}j}$ the corresponding DC link voltage, and V_j^1 the amplitude of v_j^1, where v_j^1 represents the first harmonic of ac terminal voltage v_j, synthesised by the jth H-bridge cell.

In practice, it is possible to increase the modulation index of an H-bridge cell to $(4/\pi)$, but due to incursion of H-bridge cell to the overmodulation region and the increase in current harmonics and the losses, the upper limit of the modulation index is set to one [23], i.e.

$$m_j \le 1, \quad j = 1, 2, \ldots, n \tag{2}$$

According to (2), when $m_j \le 1$, the jth H-bridge cell is in the linear modulation range; otherwise, it is in the overmodulation region and will generate some harmonics.

By writing Kirchhoff's voltage law for the ac voltage loop in Fig. 1, the following equation is derived

$$\frac{{\rm d}i_{\rm g}}{{\rm d}t} = \frac{1}{L}\left(v_{\rm g} - Ri_{\rm g} - \sum_{j=1}^{n} v_j\right) \tag{3}$$

where $i_{\rm g}$ represents the injected current to grid, $v_{\rm g}$ the grid voltage, R and L are the equivalent resistance and inductance of the input filter, and C_j is the capacitance of jth H-bridge cell. Equation (3) shows the dynamic behaviour of injected current to the grid. The Kirchhoff's current law at the DC side of the jth H-bridge cell also implies that $i_j = I_{{\rm PV}j} - i_{Cj}$ and by taking the average over it, one can obtain

$$\overline{i_j} = \overline{I_{{\rm PV}j}} - \overline{i_{Cj}} \quad \rightarrow \quad I_j = I_{{\rm PV}j} \tag{4}$$

where in (4), the capacitor average current is set to zero at steady state. If the power loss of an H-bridge cell is assumed to be zero, then the average input power and the average output power to the H-bride cell will be equal at steady state and one can write

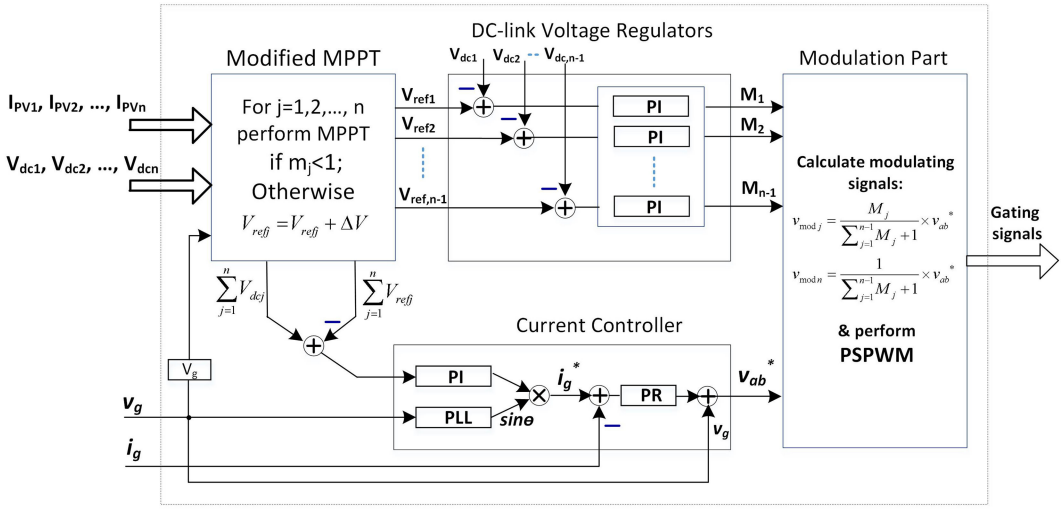

Fig. 2 *Block diagram of the control system, including the modified MPPT, individual voltage regulators, the grid current controller, and the modulation part*

$$P_{\text{in,cell}} = P_{\text{out,cell}} \quad \rightarrow \quad V_{\text{dc}j} I_{\text{h}j} = \frac{1}{2} V_j^1 I_{\text{g}} \cos\delta \tag{5}$$

where I_{g} is the amplitude of the injected current to the grid and δ represents the phase difference between the injected current i_{g} and the synthesised voltage v_j^1. Here, it is assumed that the control system operates correctly and the injected current to the grid i_{g} is sinusoidal. Generally, δ has a small value and by assuming $\cos\delta \approx 1$ and using (4), (5), and (1), the following result is obtained

$$I_{\text{PV}j} = I_j = \frac{1}{2} \frac{V_j^1}{V_{\text{dc}j}} I_{\text{g}} = \frac{1}{2} m_j I_{\text{g}} \tag{6}$$

Rewriting (6) results in

$$m_j = \frac{2 I_{\text{PV}j}}{I_{\text{g}}}, \quad j = 1, 2, \ldots, n \tag{7}$$

Moreover, at steady state, the generated average power by the PV arrays should be equal to the injected average power to the grid. Accordingly, the following result is obtained when the converter's internal loss is neglected and peak values of grid voltage and grid current are considered:

$$P = \sum_{j=1}^{n} I_{\text{PV}j} V_{\text{dc}j} = \frac{1}{2} V_{\text{g}} \cdot I_{\text{g}} \tag{8}$$

Now by inserting the value of I_{g} from (7) into (8) and calculation of m_j, the following relation is derived for the modulation index of jth H-bridge cell in the CHB inverter:

$$m_j = \frac{I_{\text{PV}j} V_{\text{g}}}{\sum_{j=1}^{n} I_{\text{PV}j} V_{\text{dc}j}} \quad \text{for } j = 1, 2, \ldots, n \tag{9}$$

It is worth noting that the value of the modulation index in (9) is calculated based on the grid peak voltage and PV arrays data which are already available for the MPPT algorithm. In contrast to (1), which needs the first harmonic of ac terminal voltage to estimate the modulation index, (9) provides a simple estimation for the modulation index based on DC values. According to (9), when the generated power by a PV array reduces, the total power [or the denominator of (9)] reduces and accordingly, the amplitude of m_j for the rest H-bridge cells will increase. As, except the array with the reduced power, the current of rest PV arrays remains constant, and therefore, the numerator of (9) does not change for those H-bridge cells while their denominators have reduced. In the worst case, when the generated power by a PV array reduces to a specific limit, the modulation index of higher-power cells may become >1 and the CHB inverter will generate a high amount of harmonics.

A reasonable way to avoid the generation of harmonics in the CHB inverter without changing the power factor is to change the operating point of H-bridge cells which are in the overmodulation region. The best solution with the minimum effect on the total generated power is to increase the DC voltage of higher-power cells (or PV arrays) gradually to the point that their modulation indices becomes one, i.e. $m_j = 1$. This idea helps to improve the performance of CHB-based PV inverters under heavy mismatching conditions.

3.2 Modified control system

The employed control system for the CHB inverter is shown in Fig. 2. This control system is made of four parts: the modified MPPT system, the grid current controller, individual DC link voltage regulators, and the modulation part. The method of current control and the DC link voltage regulation is almost similar to the presented approaches in [6, 8], but a new correction loop based on (9) is added to the tracking algorithm to extend the operating range of the CHB inverter. This extra loop keeps the CHB inverter in the linear modulation range under heavy mismatching conditions.

In the proposed control system of Fig. 2, the voltage and current of all PV arrays, grid voltage, and grid current are sampled and registered by the control system. Then, the value of the modulation index m_j for each cell is calculated sequentially according to (9). Next, the reference voltage of the jth DC link, i.e. $V_{\text{ref}j}$, is updated according to classic MPPT algorithm (P&O algorithm in this paper) if $m_j < 1$. Otherwise, the reference voltage is increased by a small step voltage, i.e.

$$V_{\text{ref}\,j} = V_{\text{ref}\,j,\,\text{old}} + \Delta V \tag{10}$$

where ΔV is the step voltage of the correction loop. It is worth mentioning that in the classic P&O algorithm, the voltage of the PV array is perturbed periodically by a small step, e.g. $\Delta V_{\text{P\&O}}$ and then the change of output power is observed. If the output power has increased, the perturbation will continue in the same direction in the next step; otherwise, it will be reversed [24]. This mechanism will be repeated by a frequency of $f_{\text{P\&O}}$ (or f_{MPPT} in this paper).

After updating the reference voltage of all H-bridge cells, they are applied to DC link voltage regulators. Since the new correction loop has been added to the MPPT algorithm, the update frequency of (10) is selected equal to the update frequency of P&O algorithm, i.e. f_{MPPT}. In addition, the step voltage of the correction loop, i.e. ΔV, is selected equal to the step voltage of P&O algorithm.

The second block in Fig. 2 is used for the control of the injected current i_{g} to the grid. In this block, the sum of DC link voltages

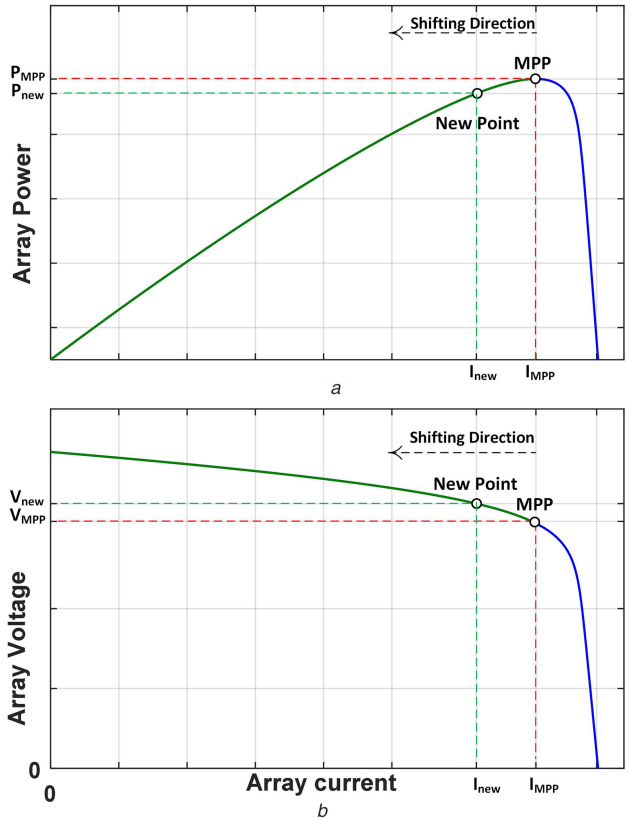

Fig. 3 *Effect of voltage increase on the operating point of PV array in the*
(a) *PI* curve,
(b) *VI* curve

($\sum_{j=1}^{n} V_{dcj}$) is compared with the sum of DC link reference voltages and the error is entered to a PI regulator. The regulator output determines the amplitude of the injected current to the grid. Then, a phase locked loop technique is utilised to synchronise the control system aiming to generate the grid current reference, i_g^*.

The ac current i_g then is compared with the reference value i_g^* and the error signal is entered to a proportional-resonant (PR) current controller [25]. The controller is tuned to control the fundamental harmonic of the current waveform. Finally, the output of the PR controller is summed with the grid voltage and is used as the reference voltage for the inverter phase voltage v_{ab}^* (or the total ac terminal voltage) and is applied to the modulation block.

The individual voltage regulators are used to regulate the voltage of separate DC links, i.e. V_{dcj} (for $j=1,2,\ldots,n-1$) to the reference voltages V_{refj} (for $j=1,2,\ldots,n-1$) generated by the modified MPPT system. Meanwhile, it is not necessary to use an additional PI regulator for the last PV array. As the voltage of last H-bridge cell is regulated automatically to V_{refn} by the control of first ($n-1$) DC links and the total voltage of DC links. Finally, the output of PI regulators, i.e. M_1, M_2,…, M_{n-1}, are used to generate the modulating signals for the H-bridge cells according to (11)

$$\begin{aligned} v_{\text{mod}j} &= \frac{M_j}{\sum_{j=1}^{n-1} M_j + 1} \times v_{ab}^*, \quad j = 1, 2, \ldots, n-1 \\ v_{\text{mod}n} &= \frac{1}{\sum_{j=1}^{n-1} M_j + 1} \times v_{ab}^* \end{aligned} \tag{11}$$

where $v_{\text{mod}1}$, $v_{\text{mod}2,\ \ldots,}$ $v_{\text{mod}n}$ are the modulating signals which are used in the PS-PWM algorithm to generate the corresponding gate signals for H-bridge cells. One should note that the modulating signals $v_{\text{mod}j}$($j=1,2,\ldots,\ n$) are derived from the output of controllers and may contain some harmonics due to the ripple of DC links, distortion of grid current, and operation of CHB inverter in the overmodulation region. Hence, the modulating signals $v_{\text{mod}j}$ cannot be employed for the calculation of modulation indices as stated in (1).

The last point in the modified tracking system is related to the value of step voltage ΔV in (10). Since the affecting parameter on the performance of control system is the product of update frequency (f_{MPPT}) and the step voltage, first an upper limit is derived for it. To achieve this goal, the settling time (t_{settle}) of the DC link is determined when a step disturbance is applied to the reference voltage of DC links. In this evaluation, a 10% step voltage (or 0.1 V_{mpp}) is applied and the upper limit is determined by

$$f_{\text{MPPT}} \times \Delta V < \frac{0.1\ V_{\text{mpp}}}{t_{\text{settle}}} \tag{12}$$

In (12), if the upper limit is not satisfied, the system will not reach a steady state and undesirable oscillations may appear on DC link voltages. Meanwhile, choosing a very small value for $f_{\text{MPPT}} \times \Delta V$ will lead to a slow transient response which is also undesirable. Hence, it is proposed to use a value of one-third to one-fifth of the right term in (12). Moreover, the MPPT frequency is chosen lower than the PWM carrier frequency, e.g. one-fifth of the carrier frequency.

3.3 Effect of voltage increase on the total power generation

As stated before, when the PV arrays (or H-bridge cells) in the CHB inverter have asymmetric operating conditions, the modulation indices of higher-power cells may become >1. In this case, the presented controller in Fig. 2 will increase the voltage of those H-bridge cells beyond the MPP voltage. Hence, the total generated power will reduce.

As a case study, it is assumed that there is a CHB inverter with n separate PV arrays, where the irradiance level of the first PV array is much lower than the irradiance levels of rest ($n-1$) PV arrays. In addition, it is assumed that the rest ($n-1$) PV arrays (or H-bridge cells) have identical operating conditions. In this case, depending on the grid voltage, the higher-power cells may enter to the overmodulation region and generate harmonics. To bring these H-bridge cells back to the linear modulation range, their operating voltages should be increased [or equivalently their operating points should be shifted to the left side of MPP in the corresponding power–current (*PI*) curve, as it is shown in Fig. 3 for a sample PV array]. The voltage increase is stopped when the H-bridge cells reach the condition $m_j=1$, $j=2,\ 3,\ldots,n$. Now, the following equation can be written for the modulation index of higher-power cells, before applying the modified algorithm

$$\frac{I_{\text{mpp}} \times V_{\text{g}}}{P_{1\text{mpp}} + (n-1)P_{\text{mpp}}} = m_j > 1 \quad \text{for } j = 2, 3, \ldots, n \tag{13}$$

where $P_{1\text{mpp}}$ represents the generated power by the first PV array at the MPP and (I_{mpp}, P_{mpp}) corresponds to the MPP point of the rest PV arrays. After applying the proposed strategy, the new operating point of higher-power cells will change to (I_{new}, P_{new}) to meet the condition $m_j=1$ for $j=2,3,\ldots,n$. In this case, the following equation can be written for higher-power cells:

$$\frac{I_{\text{new}} \times V_{\text{g}}}{P_{1\text{mpp}} + (n-1)P_{\text{new}}} = 1 \tag{14}$$

Now to find the value of I_{new} (or P_{new}) in (14), one has to substitute the power value as a function of array current. To achieve this goal, the left side of the *PI* curve in Fig. 3*a* (green part) is approximated by a third-order polynomial, i.e.

$$P(I) = aI^3 + bI^2 + cI + d \quad \text{(left side of MPP)}$$

(15) where a, b, c, and d are the coefficients of the fitted polynomial to the left side of the *PI* curve in Fig. 3*a*. One should note that the polynomial coefficients should be updated when the

temperature or irradiance level changes; otherwise, the estimation will have some errors. Now by substituting the value of V_g from (13), and $P(I_{new})$ from (15), into (14), the following equation is derived

$$aI_{new}^3 + bI_{new}^2 + \left(c - \frac{P_{mpp} + (p_{1mpp}/n-1)}{I_{mpp}} m_j\right) I_{new} + \left(d + \frac{p_{1mpp}}{n-1}\right) = 0 \quad (16)$$

In (16), the only unknown variable is I_{new} which can be derived from solving the equation. The acceptable answer is the nearest real root to I_{MPP}. After finding I_{new}, P_{new} can be calculated from (15) and the power change is determined by (17)

$$\Delta P_{total} = (n-1)(P_{mpp} - P_{new}) \quad (17)$$

One should note that the above calculation is valid for the assumed case study. In any other cases, a similar approach can be taken to derive the analytical formula.

To have a better sense about the amount of power reduction as a function of irradiance change, the following example is considered.

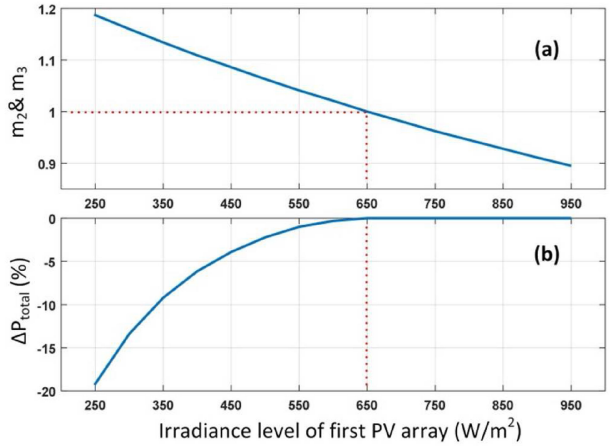

Fig. 4 *Variation of irradiance level in the first PV array when the second and third ones are constant in the seven-level CHB inverter*
(a) Corresponding modulation indices of higher-power cells,
(b) Percentage of power reduction

It is assumed that there is a seven-level CHB inverter with three H-bridge cells, where each H-bridge is connected to a PV array. The PV arrays themselves are made of eight series-connected PV modules with the given parameters in Table 1. Furthermore, it is assumed that the irradiance level of all PV arrays is 950 W/m^2 at first and the temperature is 60°C for all PV arrays. Then, the irradiance level of the first PV array is reduced from 950 to 250 W/m^2 and the amount of power reduction is calculated by (16) and (17) and demonstrated in Fig. 4*b*. It is seen that the second and third H-bridge cells enter to the overmodulation region when the irradiance level of the first PV array becomes lower than 650 W/m^2.

4 Simulation results

In this section, the performance of modified control system for the CHB inverter is verified in Matlab/Simulink environment. The selected inverter for study is a single-phase seven-level CHB inverter and the control system is similar to Fig. 2. The utilised parameters for the CHB inverter, the controllers, and PV modules are demonstrated in Table 1. In the following investigations, eight series-connected modules from Yingli Solar ($V_{oc} = 22.28$, $I_{sc} = 4.15$, $P_{max} = 70$ W) are used as a PV array to feed one DC link, and therefore, in total, 24 modules are used. Moreover, the solar modules are modelled based on single-diode model and P&O algorithm is employed for the MPPT goal [24].

4.1 Comparative investigation of modified control system

In this simulation, it is assumed that the irradiance level of the first PV array is 550 W/m^2 and the second and third ones are 950 W/m^2. In addition, the temperature of all PV arrays is 60°C and the amplitude of the grid voltage is 330 V. The simulations are carried out to compare the behaviour of the control system, before and after applying the modified control system. In fact, in all simulations, the controller first works based on the proposed algorithm in [6] for $t < 1.5$ s, but at $t = 1.5$ s, the new strategy is applied to the control system and its behaviour is investigated.

Fig. 5 shows the waveform of the injected current i_g to the grid for the whole period. A zoomed view of the current waveform, before and after applying the proposed strategy, is shown in Figs. 5*a* and *b*, respectively. FFT analysis for Fig. 5*a* reveals that the THD value is ∼12.5%, before applying the proposed idea. This is mainly due to operation of second and third H-bridge cells in the

Table 1 Utilised system parameters in the simulation study

Parameter	Symbol	Value
number of H-bridge cells	n	3
amplitude of grid voltage	V_g	330 V
total Power at STC	P_{nom}	1680 W
inductor value	L	4.4 mH
Dc link capacitance	C_j	1 mF
step voltage in the P&O and the correction loop	ΔV	0.03 V
MPPT frequency	f_{mppt}	1 kHz
carrier frequency	f_{cr}	5 kHz
individual voltage regulators	K_p	0.00025
	K_i	0.25
PR current controller	K_p	120
	K_i	3000
voltage regulator of current loop	K_p	0.0001
	K_i	4
diode saturation current	I_{s0}	1.45 nA
diode quality factor	η	1.11
series resistance	R_s	0.418 Ω
parallel resistance	R_p	87 Ω
number of series cells	m	36

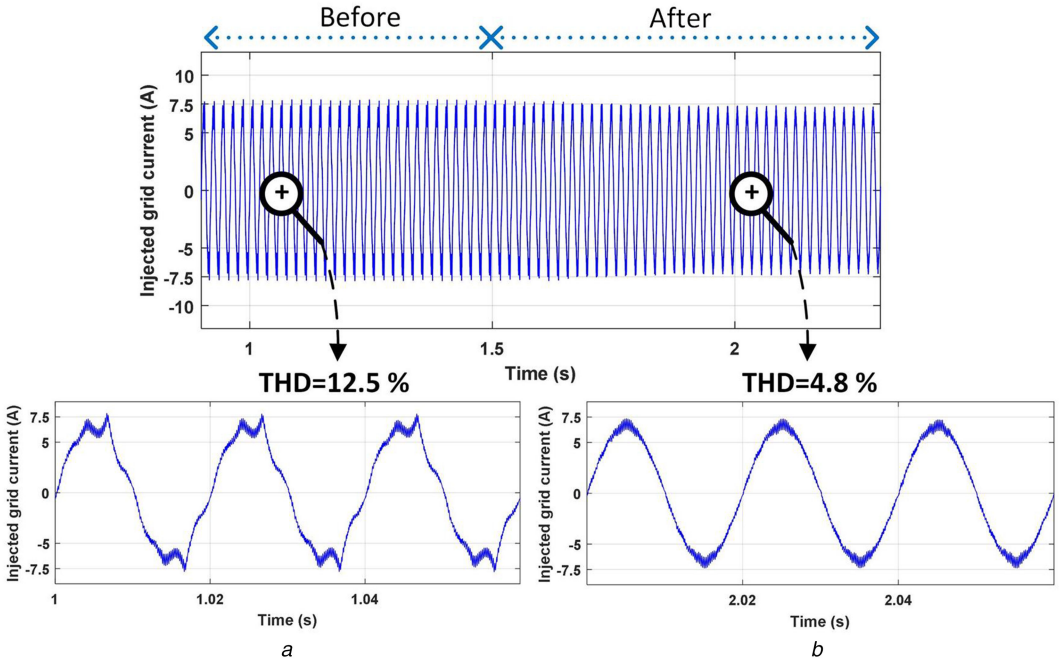

Fig. 5 *Injected current to grid*
(a) By the presented algorithm in [6],
(b) By the proposed strategy in this paper

overmodulation region. This fact can be predicted by the defined modulation indices in (9), i.e. m_2 and m_3 and also the demonstrated curve in Fig. 4*a*. It is evident that for $t < 1.5$ s, the amplitude of m_2 and m_3 is >1 and therefore, the CHB inverter generates harmonics. In this condition, the controllers do not operate correctly and the modulating signals to the PS-PWM block are distorted significantly. However, as it is shown in Fig. 6*a*, after applying the proposed strategy, the modulation indices are reduced to 1 and the CHB inverter can operate correctly.

To better understand the behaviour of the control system, the modulating waveforms and DC link voltages (and the corresponding reference values) are shown in Figs. 6*b* and *c*, respectively. From Fig. 6*b*, it is seen that the modulating waveforms are not sinusoidal due to improper operation of the control system. However, when the new strategy is applied, the modulating waveforms are corrected as sinusoidal waveforms. Then, the PWM modulator will synthesise the sinusoidal waveforms and lower harmonics will be generated. From Fig. 6*c*, it is seen that DC link voltages are regulated to $V_{dc1} = 121$, $V_{dc2} = 122$, and $V_{dc3} = 122$ V before $t = 1.5$ s. However, after applying the proposed strategy, DC voltages of second and third H-bridge cells become 128 V, while the voltage of the first cell does not change. This result shows the correct behaviour of controller in increasing the voltage of higher-power cells to bring them back to the linear modulation range.

Fig. 6*d* shows the amount of the injected power to the grid in the above simulation. It is seen that the total generated power reduces from 1112 to 1100 W or ∼1.07%. Hence, by reduction in generated power for ∼1%, the inverter interruption and its isolation from the grid is avoided. The amount of power reduction is also predictable from the demonstrated curve in Fig. 4. According to Fig. 4, when the solar irradiance of the first PV array is 550 W/m^2, the modulation indices of second and third cells are $m_2 = m_3 = 1.041$ and the total amount of power reduction is ∼1.09%. Hence, there is a good agreement between the theory and simulation result.

4.2 Dynamic performance of control system

The dynamics of CHB-based PV system generally come from two perspectives – solar irradiance change and grid voltage variation. Thus, two simulations are provided to study the dynamic behaviour of the proposed control system. In the first investigation, the irradiance level of all PV arrays is equal to 950 W/m^2 at first. Then, at $t = 1.5$ s, the irradiance level of the first PV array reduces from 950 to 550 W/m^2 in a stepwise manner and returns to the initial value at $t = 2.5$ s. Fig. 7 shows the obtained results for the DC-link voltage waveforms and the injected current to the grid under this variation. It is seen that the corresponding undershoot/overshoot of DC-link voltages is <20% and settling time is almost 0.35 s for DC link voltages. Moreover, the transient time of the third DC link is larger than other links due to indirect voltage regulation of the third cell. It is also seen that the behaviour of the injected current to the grid is smooth and the settling time is <0.15 s.

In the second investigation, the irradiance level of the first PV array is 550 W/m^2, the second and third ones are 950 W/m^2, and the peak of the grid voltage is 330 V. Then, at $t = 1.5$ s, the grid voltage increases 10% in a stepwise manner and returns to the initial value at $t = 3$ s. Fig. 8 shows the startup, steady state, and dynamic behaviour of the CHB inverter under this test condition.

Evaluation of Fig. 8 reveals that the inverter well behaves at the startup condition and all DC links reach the steady-state condition in <0.8 s. Since the third DC-link is regulated indirectly, its transition time takes more than other cells. Moreover, according to (9), with the increase in grid voltage, the modulation index of H-bridge cells increases and as the second and third PV arrays are already at the border value of the modulation index, the control system increases their reference voltages from 128 to 138 V. By noting to the step voltage of 0.03 V and the update frequency of 1 kHz, 0.33 s will be needed for the update of reference voltages, which is also confirmed in Fig. 8. The bottom waveform in Fig. 8 shows the smooth behaviour of the injected current to the grid at startup and transient conditions. One has to note that a CHB inverter with the conventional control system will show undesirable behaviour under such dynamic condition and it may become unstable.

5 Experimental results

In the experimental investigation, a seven-level CHB inverter and a TMS-F28335 DSP control board are used to verify the validity of new control strategy. Fig. 9 shows the photo of laboratory prototype and PV panels utilised for the experimental investigation. To have a fair comparison, the type of PV panels and the size of arrays are selected similar to the simulation study. In addition, the same inverter parameters and grid voltage are utilised for the experimental tests. However, there are some differences in the

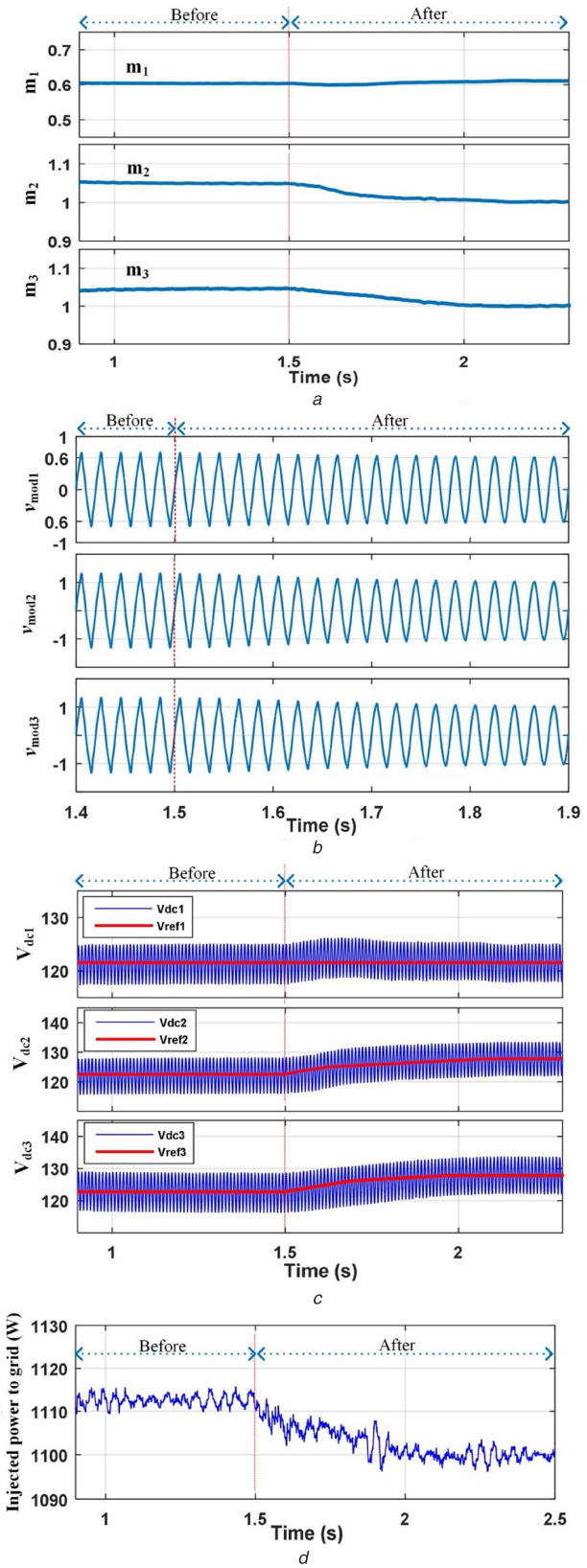

Fig. 6 *Evaluation of proposed control system behaviour before and after applying the new strategy*

(a) Modulation indices,

(b) Modulating waveforms,

(c) Arrays DC link voltages and reference values,

(d) Total injected power to the grid

control system parameters which are listed in Table 2. This is mainly due to some differences between the utilised model in the simulation and the practical system. For example, non-linearity of

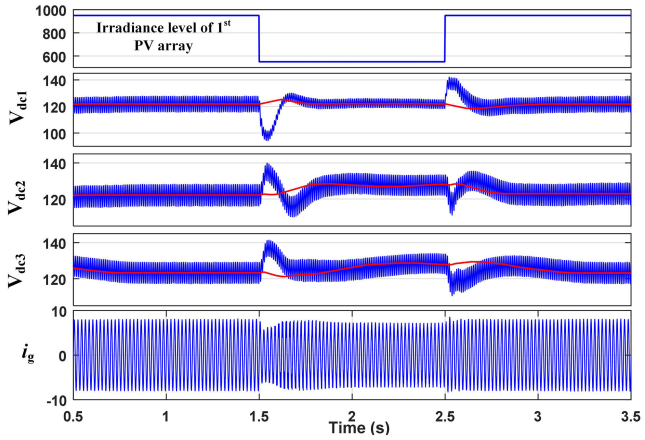

Fig. 7 *Dynamic behaviour of the proposed control system under change of irradiance level of the first PV array*

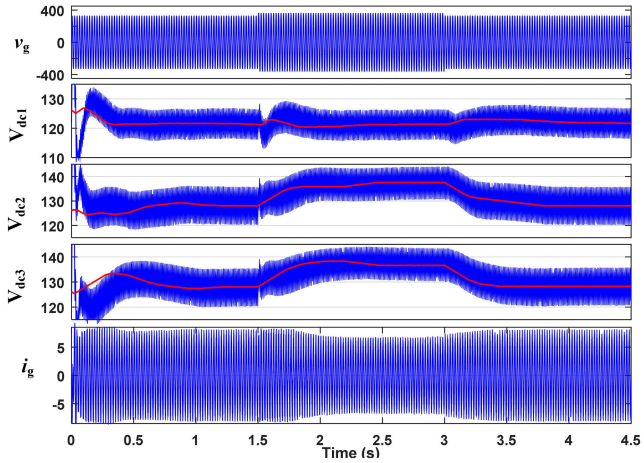

Fig. 8 *Dynamic behaviour of the proposed control system under grid voltage swell and non-uniform distribution of irradiances*

inductor, sampling delays, cable and connection losses, and the series reactance of grid are the main sources of differences.

For the experimental investigation, three mechanical structures have been implemented with the adjustable angles for PV panels. Using this flexibility, one can adjust the irradiance level of each array. For example, in the following test, the angle of the first PV array is set to 90° and the second and third ones are set to 30°, which can be seen in Fig. 7. The measured temperature of PV arrays is also 60°C.

Same as the simulation, the presented approach in [6] is applied to the CHB inverter at first. Owing to asymmetric condition, the second and third H-bridge cells are entered to the overmodulation region. The new strategy then is applied and the corresponding DC link voltages and grid current are recorded and shown in Fig. 10*a*. Moreover, Figs. 10*b* and *c* show the steady-state behaviour of the system before and after applying the new strategy.

Evaluation of Fig. 10*a* shows that the transient time of DC link voltages is ∼250 ms which is in good agreement with the simulation result in Fig. 6*b*. Furthermore, according to steady-state responses in Figs. 10*b* and *c*, the voltage of the first DC link does not change at steady state, while the voltages of second and third PV arrays are increased from 121 and 117 to 135 and 131 V, respectively. This action is taken by the controller to keep the H-bridge cells in the linear modulation range and to decrease the harmonic content. The small difference between the DC link voltages of second and third PV arrays is due to some tolerances of the PV arrays and the angle of structures.

Finally, the recorded data of grid current and grid voltage have been imported to Matlab/Simulink environment to extract the corresponding RMS and THD values, before and after applying the new strategy. The evaluation shows that the current THD reduces from 14.3 to 5% after applying the proposed strategy. Moreover,

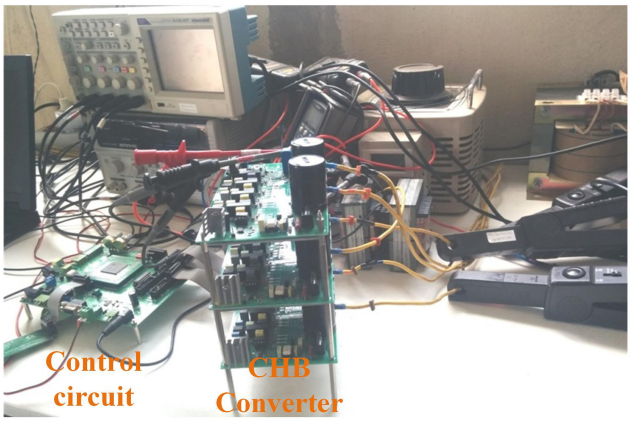

a

b

Fig. 9 *Photo of*
(a) Laboratory prototype,
(b) Utilised PV panels

Table 2 Utilised control system parameters in the experimental investigation

Parameter	Symbol	Value
step voltage in the P&O and the correction loop	ΔV	0.03 V
update and MPPT frequency	f_{mppt}	1 kHz
carrier frequency	f_{cr}	5 kHz
individual voltage regulators	K_p	0.0001
	K_i	0.1
PR current controller	K_p	130
	K_i	1000
voltage regulator of current loop	K_p	0.0005
	K_i	1.2

the total generated power reduces from 1152 to 1140 W which is <1%. The obtained experimental results are in good agreement with the simulation results and confirm the correct behaviour of the proposed strategy.

6 Conclusion

In this paper, a modified control strategy was proposed for the CHB inverter in the grid-connected PV applications. Based on the circuit analysis, a mathematical relation was derived for determination of cells' operating conditions in the CHB inverter. This relation shows the value of cells' modulation indices based on the PV system data. Accordingly, a modified control strategy was proposed to extend the operating range of the CHB inverter under heavy mismatching conditions. In this method, the condition of each H-bridge is checked continuously and when a cell enters to the overmodulation region, its voltage is gradually increased to bring it back to the linear region. This modification helps to prevent the interruption of CHB inverter due to extra harmonic

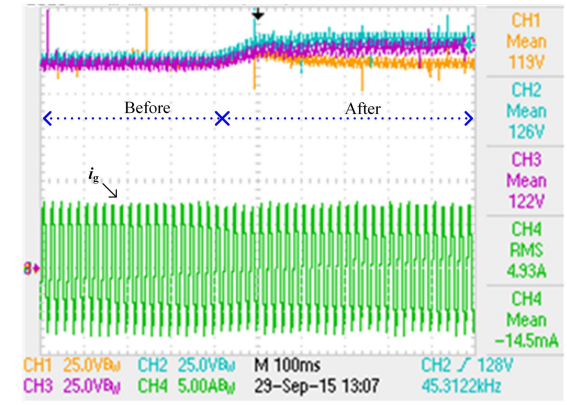

a

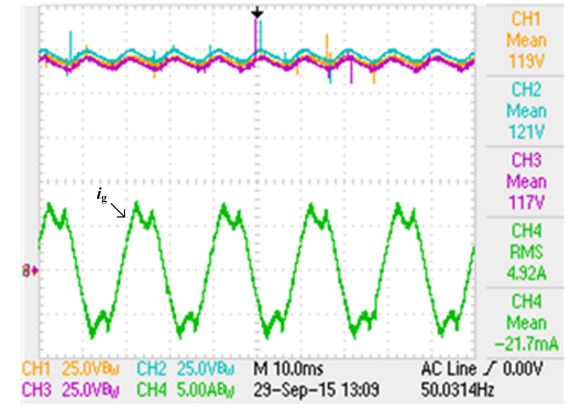

b

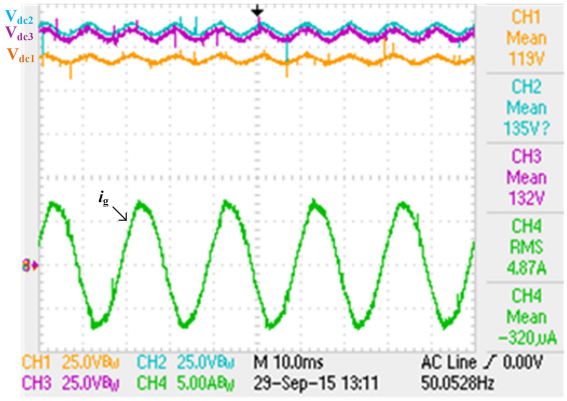

c

Fig. 10 *DC-link voltage waveforms and grid current in experimental test*
(a) System behaviour at the instant of applying the proposed strategy,
(b) Zoomed-view of waveforms before applying the proposed strategy,
(c) Zoomed-view of waveforms after applying the proposed strategy

generation in the overmodulation region. The proposed method can be easily applied to the already existing control systems to increase their operating range under asymmetric conditions.

7 References

[1] Kouro, S., Malinowski, M., Gopakumar, K., *et al.*: 'Recent advances and industrial applications of multilevel converters', *IEEE Trans. Ind. Electron.*, 2010, **57**, (8), pp. 2553–2580

[2] Bedram, A., Davoudi, A., Balog, R.S.: 'Control and circuit techniques to mitigate partial shading effects in photovoltaic arrays', *IEEE J. Photovolt.*, 2012, **2**, (4), pp. 532–546

[3] Hajizadeh, M., Fathi, S.H.: 'Fundamental frequency switching strategy for grid-connected cascaded H-bridge multilevel inverter to mitigate voltage harmonics at the point of common coupling', *IET Power Electron.*, 2016, **9**, (12), pp. 2387–2393

[4] Kouro, S., Leon, J.I., Vinnikov, D., *et al.*: 'Grid-connected photovoltaic systems: an overview of recent research and emerging PV converter technology', *IEEE Ind. Electron. Mag.*, 2015, **9**, (1), pp. 47–61

[5] Oliveira, F.M., Oliveira da Silva, S.A., Durand, F.R., *et al.*: 'Grid-tied photovoltaic system based on PSO MPPT technique with active power line conditioning', *IET Power Electron.*, 2015, **9**, (6), pp. 1180–1191

[6] Villanueva, E., Correa, P., Rodriguez, J., *et al.*: 'Control of a single-phase cascaded H-bridge multilevel inverter for grid-connected photovoltaic systems', *IEEE Trans. Ind. Electron.*, 2009, **56**, (11), pp. 4399–4406
[7] Cecati, C., Ciancetta, F., Siano, P.: 'A multilevel inverter for photovoltaic systems with fuzzy logic control', *IEEE Trans. Ind. Electron.*, 2010, **57**, (12), pp. 4115–4125
[8] Kouro, S., Wu, B., Moya, A., *et al.*: 'Control of a cascaded H-bridge multilevel converter for grid connection of photovoltaic systems'. 35th Annual Conf. on Industrial Electronics (IECON '09), 2009, pp. 3976–3982
[9] Xiao, B., Hang, L., Mei, J., *et al.*: 'Modular cascaded H-bridge multilevel PV inverter with distributed MPPT for grid-connected applications', *IEEE Trans. Ind. Appl.*, 2015, **51**, (2), pp. 1722–1731
[10] Kumar, N., Saha, T.K., Dey, J.: 'Sliding-mode control of PWM dual inverter-based grid-connected PV system: modeling and performance analysis', *IEEE J. Emerg. Sel. Topics Power Electron.*, 2016, **4**, (2), pp. 435–444
[11] Farivar, G., Hredzak, B., Agelidis, V.: 'A dc-side sensorless cascaded H-bridge multilevel converter based photovoltaic system', *IEEE Trans. Ind. Electron.*, 2016, **63**, (7), pp. 4233–4241
[12] Chavarria, J., Biel, D., Guinjoan, F., *et al.*: 'Energy-balance control of PV cascaded multilevel grid-connected inverters under level-shifted and phase-shifted PWMs', *IEEE Trans. Ind. Electron.*, 2013, **60**, (1), pp. 98–111
[13] Cortes, P., Kouro, S., Barrios, F., *et al.*: 'Predictive control of a single-phase cascaded H-bridge photovoltaic energy conversion system'. 7th Int. Power Electronics and Motion Control Conf. (IPEMC), 2012, pp. 1423–1428
[14] Rezaei, M., Iman-Eini, H., Farhangi, S.: 'Grid-connected photovoltaic system based on a cascaded H-bridge inverter', *J. Power Electron.*, 2012, **12**, (4), pp. 578–586
[15] Eskandari, A., Javadian, V., Iman-Eini, H., *et al.*: 'Stable operation of grid connected cascaded H-bridge inverter under unbalanced insolation conditions'. 3rd Int. Conf. on Electric Power and Energy Conversion Systems, 2013, pp. 1–6
[16] Iman-Eini, H., Amini, M., Farhangi, Sh.: 'Improving the performance of grid-connected cascaded H-bridge photovoltaic inverters under asymmetric insolation conditions', *Iranian J. Electr. Comput. Eng.*, in Persian language, 2015, **13**, (2), pp. 135–142
[17] Miranbeigi, M., Iman-Eini, H.: 'Hybrid modulation technique for grid-connected cascaded photovoltaic systems', *IEEE Trans. Ind. Electron.*, 2016, **63**, (12), pp. 7843–7853
[18] Liu, L., Li, H., Xue, Y., *et al.*: 'Reactive power compensation and optimization strategy for grid-interactive cascaded photovoltaic systems', *IEEE Trans. Power Electron.*, 2015, **30**, (1), pp. 188–202
[19] Liu, L., Li, H., Xue, Y., *et al.*: 'Decoupled active and reactive power control for large scale grid-connected photovoltaic systems using cascaded modular multilevel converters', *IEEE Trans. Power Electron.*, 2015, **30**, (1), pp. 176–187
[20] Bacha, S., Picault, D., Burger, B., *et al.*: 'Photovoltaics in microgrids: an overview of grid integration and energy management aspects', *IEEE Ind. Electron. Mag.*, 2015, **9**, (1), pp. 33–46
[21] Malinowski, M., Gopakumar, K., Rodriguez, J., *et al.*: 'A survey on cascaded multilevel inverters', *IEEE Trans. Ind. Electron.*, 2010, **57**, (7), pp. 2197–2206
[22] Yang, Y., Zhou, K., Blaabjerg, F.: 'Current harmonics from single-phase grid-connected inverters, examination and suppression', *IEEE J. Emerg. Sel. Topics Power Electron.*, 2016, **4**, (1), pp. 221–233
[23] Zhou, K., Wang, D.: 'Relationship between space-vector modulation and three-phase carrier-based PWM: a comprehensive analysis', *IEEE Trans. Ind. Electron.*, 2002, **49**, (1), pp. 186–196
[24] Hussein, K.H., Muta, I., Hoshino, T., *et al.*: 'Maximum photovoltaic power tracking: an algorithm for rapidly changing atmospheric conditions', *IEE Proc. Gener. Transm. Distrib.*, 1995, **14**, (1), pp. 59–64
[25] Eha, H., Vu, T.K., Kim, J.E.: 'Design and control of proportional- resonant controller based on photovoltaic power conditioning system'. IEEE Energy Conversion Congress and Exposition, 2009, pp. 2198–2205